CHEMISTRY & SUSTAINABILITY

CHEMSUSCHEM

ENERGY & MATERIALS

Accepted Article

Title: Pyran-bridged indacenodithiophene: A novel building block for constructing efficient A-D-A type nonfullerene acceptor for polymer solar cells

Authors: Renqiang Yang, Shuguang Wen, Yao Wu, Yingying Wang, Yi Li, Ling Liu, Huanxiang Jiang, and Zhitian Liu

To be cited as: *ChemSusChem* 10.1002/cssc.201701917

Link to VoR: http://dx.doi.org/10.1002/cssc.201701917

A Journal of

ChemPubSoc Europe

WILEY-VCH

www.chemsuschem.org

10.1002/cssc.201701917

WILEY-VCH

Pyran-bridged indacenodithiophene: A novel building block for constructing efficient A-D-A type nonfullerene acceptor for polymer solar cells

Shuguang Wen,[a] Yao Wu,[b] Yingying Wang,[a] Yi Li,[a] Ling Liu,[a] Huanxiang Jiang,[a] Zhitian Liu*[b], and Renqiang Yang*[a]

S. Wen and Y. Wu contributed equally to this work.

Abstract: In recent years, nonfullerene acceptors have attracted much attention due to their great potential for achieving high performance polymer solar cells. In this paper, a novel ladder type building block of pyran-bridged indacenodithiophene (PDT) has been designed for constructing A-D-A nonfullerene acceptors through introducing oxygen atoms into the commonly used indacenodithiophene (IDT) unit. The key step for the synthesis of PDT unit is accomplished by a BBr_3-mediated tandem cyclization-deprotection reaction to construct the pyran-ring. In this approach, a novel molecular acceptor PTIC was successfully synthesized and applied in polymer solar cell device. Compared to the IDT-based acceptor, PTIC exhibits higher HOMO levels and wider optical bandgap at 550-800 nm. Polymer solar cells devices fabricated with PBDB-T:PTIC as active layer show a power conversion efficiency (PCE) of 7.66%. The introduction of oxygen atoms would be an effective approach for the modification of acceptor materials for polymer solar cells.

Introduction

Polymer solar cells (PSCs) have attracted extensive attention in the past decades due to the advantages of light weight, low cost and flexibility.[1-6] Fullerene derivatives are usually used as electron acceptors in the blend film of bulk heterojunction (BHJ) structure because of their good electron affinity and mobility. However, the intrinsic drawbacks limit their photovoltaic performance, such as weak optical absorption, difficult structure modification and high production cost.[7] As a replacement of fullerene derivatives, Zhan's group has developed a series of A-D-A type molecules as nonfullerene acceptor with indacenodithiophene (IDT) as the core structure.[8] These acceptors showed great potential to outperform fullerene and its derivatives. The power conversion efficiencies (PCEs) of organic solar cells devices based on these nonfullerene acceptors have exceeded 13%.[9] Recent years' research has witnessed rapid progress of these acceptors for their highly tunable physical and photoelectric properties by changing the donor unit, end-capping acceptor unit, side chains or π-bridge units, which inspires the development of their donor counterparts at the same time.[10] Importantly, it's easy for these nonfullerene acceptors to modulate the bandgaps, which is in favor of expanding optical absorption and enables application in semitransparent organic solar cells.[11]

The donor unit is core structure of A-D-A type nonfullerene acceptors, which plays a vital role in adjusting highest occupied molecular orbital (HOMO) levels, charge mobility and aggregations behaviors. There are many good results obtained by modifying the donor units including IDT,[12-16] IDTT,[9,17] IBDT,[18] DTCC,[19] BT,[20-22] et al. For example, Zhan's group reported IBDT as the donor unit by π-extending the IDTT core with thiophene units.[18] IBDT has larger rigid and coplanar structure and stronger electron-donating ability, which is in favor of enhancing the absorption and charge transport. The end-groups have significant effect on lowest unoccupied molecular orbital (LUMO) levels and molecular packing behaviors. These nonfullerene acceptors were usually end-capped with IC,[19,23,24] fluorinated IC,[9,25] methylated IC,[26] thienyl-fused indanone,[17,27] rhodamine[14,28] et al. Hou et al. reported the acceptor material of ITCC with thienyl-fused indanone as end groups.[17] This molecular showed higher LUMO level, closer π-π stacking distance and higher electron mobility than that of ITIC. The side chains are essential components of nonfullerene acceptors to guarantee solubility, modulate aggregation behaviors and adjust energy levels, which includes hexylphenyl,[29,30] hexylthienyl,[21] hexylselenophenyl,[31] and alkyl side chains[32-34]. And π bridges were usually incorporated to elongate π-conjugation length, such as benzothiazole,[28] thiophene,[35,36] diketopyrrolopyrrole,[14] thiazole,[37] et al. Since the nonfullerene acceptors have excellent flexibility in structure modification and great potential to achieve high efficiency, much more efforts can be done to optimize the chemical structure.

In order to improve the performance of PSC, it's an important strategy to expand the optical absorption range, which can be realized by lowering LUMO level or enhancing HOMO level. However, low LUMO level of acceptor would result in reduced open circuit voltage (V_{OC}) of device. So appropriately enhancing the HOMO level is a reasonable approach to expand optical absorption range. Herein, we have designed and synthesized a novel nonfullerene acceptor of PTIC, which has a pyran-bridged indacenodithiophene (PDT) as donor unit and is end-capped by 1, 1-dicyanomethylene-3-indanone groups. The incorporation of oxygen atoms is in favor of increasing HOMO level and reducing the band gap. As a result, this material shows a narrow band gap of 1.55 eV and broad absorption throughout visible and near

[a] Dr. S. Wen, Y. Wang, Y. Li, L. Liu, H. Jiang, Prof. R. Yang
CAS Key Laboratory of Bio-based Materials
Qingdao Institute of Bioenergy and Bioprocess Technology, Chinese Academy of Sciences, Qingdao 266101, China
E-mail: yangrq@qibebt.ac.cn
[b] Y. Wu, Prof. Z. Liu
School of Materials Science & Engineering, Wuhan Institute of Technology, Wuhan 430205, China
E-mail: able.ztliu@wit.edu.cn

Supporting information for this article is given via a link at the end of the document.

infrared region (500-800 nm). Crystal structure of PDT indicates that an ordered molecular packing is formed, which is in favor of charge transport in the film. PSC devices were fabricated employing PTIC as acceptor and PBDB-T as donor material. Power conversion efficiency of 7.66% was achieved with V_{OC} of 0.84 V, J_{SC} of 14.2 mA cm^{-2} and FF of 0.64. This research indicates that the introduction of oxygen group to IDT unit is an important strategy for the modification of acceptor materials.

Results and Discussion

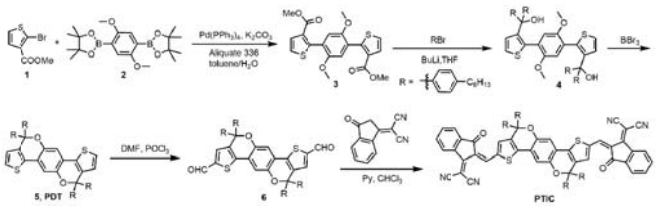

Scheme 1. Synthetic route of small molecular acceptor PTIC.

Material synthesis

The synthesis of PTIC is started from Suzuki coupling reaction of bromide **1** and borated **2** to produce compound **3**. Then the side chains of 4-hexylphenyl group were introduced to give compound **4**. With **4** in hand, compound **5** (PDT) was successfully obtained by BBr_3 initiated tandem cyclization/deprotection reaction in high yield. After two aldehyde groups were introduced, the terminal group of 2-(3-oxo-2, 3-dihydroinden-1-ylidene)-malononitrile were reacted with the aldehyde **6** to afforded the final product PTIC. The detailed synthetic procedures can be found in Supporting Information.

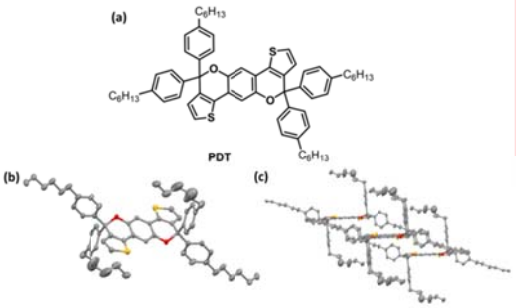

Figure 1. (a) Chemical structure of PDT core; (b) geometric structure of PDT; (c) stacking of PDT in one crystal cell.

Single crystal is an important approach for the investigation of molecular packing in the blend film of PSCs. However, there's no report about the crystal structure of acceptors such as ITIC, because the core structure of IDTT is segregated each other by the lateral four 4-hexylphenyl groups. We have fortunately obtained the single crystal of key intermediate PDT, so the chemical structure can be definitely determined by X-ray structure analysis (Figure 1). Importantly, it is shown that the central backbone is nearly planar and parallel to each other. Four lateral 4-hexylphenyl groups are not symmetrically distributed to the two sides of backbone, but two of them are perpendicular to the backbone and two are nearly in the backbone plane. So the molecules form a very ordered close slip-stacked packing in crystals, which is reported to prevent the excimer formation and reduce geminate recombination.[38] According to this result, the molecule of PTIC is deduced to form a more ordered packing structure than the acceptors derived from IDT.

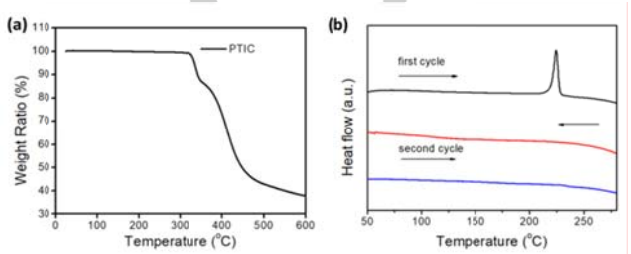

Figure 2. (a) TGA curve of PTIC; (b) DSC thermogram of PTIC upon first and second heating and cooling cycles.

Thermal properties

The thermal properties of PTIC were investigated using thermogravimetric analysis (TGA) and differential scanning calorimetry (DSC). As depicted in Figure 2, the decomposition temperatures (Td) with 5% weight loss were observed at 334 °C. PTIC exhibits good thermal stability which meets the temperature requirement for practical photovoltaic application. The DSC scan of neat PTIC from 50 to 270 °C with 10 °C/min was exhibited in Figure 2b. A sharp melting endothermic transition around 220 °C can be observed, which indicates that PTIC is highly crystalline due to its structural planarity as deduced from above X-ray structure analysis. Upon the cooling cycle after melting, no recrystallization peak is observed, suggesting the material appears to become kinetically trapped in the amorphous phase.[39] On the second cycle of heating, no peak can be found, signifying a feature of amorphous material. In the first heating and cooling scan, the crystallinity of PTIC is broken, so no melting transition is observed in the second heating scan.

Optical and electronic properties

As shown in Figure 3, PTIC showed absorption ranging from 550 nm to 800 nm. Li et al. have reported the acceptor of IDT-IC based on IDT core structure that showed absorption spectrum range from ca. 520 nm to 720 nm.[24] Compared to IDT-IC, PTIC had broader and redshifted absorption. Besides, the molar extinction coefficient of PTIC was as high as 8.8×10^4 M^{-1} cm^{-1}. The broad and near-infrared absorption with high extinction coefficient is beneficial for photocurrent generation in active layer. Compared to the absorption of PTIC in chloroform solution, the maximum absorption peak in solid state red-shifted about 67 nm, which means strong aggregation in PTIC solid film. Interestingly, the onset of the absorption in blend film blue-shifted 35 nm compared to the absorption in pure PTIC film,

which suggests that the packing of PTIC in the blend film might be disrupted by donor material.

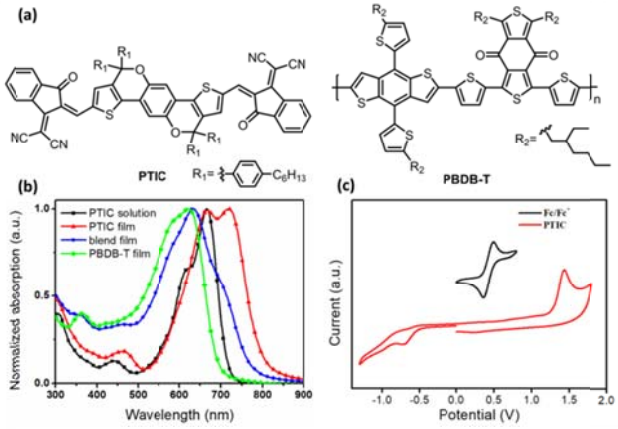

Figure 3. (a) Chemical structures of PTIC and PBDB-T; (b) absorption spectra of PTIC in $CHCl_3$ solution, pristine film, and blend film of PTIC:PBDB-T (1:1); (c) cyclic voltammetry curve of PTIC.

Table 1. Optical and electrochemical properties of PTIC.

Molecule	λ_{sol} [nm]	λ_{film} [nm]	λ_{onset} [nm]	ε_{max} [M^{-1} cm^{-1}]	E_g^{opt} [eV]	HOMO [eV]	LUMO [eV]
PTIC	667	676, 734	800	8.8×10^4	1.55	-5.67	-3.85

The energy levels of PTIC is determined by cyclic voltammetry (CV) with films on the gold electrode in an acetonitrile solution of 0.1 mol L^{-1} Bu_4NPF_6 using ferrocene (-4.8 eV) as standard reference (Table 1). The redox potential of the Fc/Fc^+ internal reference is 0.43 V *vs.* SCE. The LUMO level is determined by $E_{LUMO} = -e(E_{Red} + 4.8 - E_{1/2,(Fc/Fc+)})$ and the HOMO level is determined by $E_{HOMO} = -e(E_{ox} + 4.8 - E_{1/2,(Fc/Fc+)})$. The onset reduction potential of PTIC is -0.52 V. Hence, the LUMO level is -3.85 eV. Accordingly, the HOMO level was determined to be -5.67 eV. The ΔHOMO and ΔLUMO level of PBDB-T:PTIC are larger than 0.3 eV,[40] which can guarantee the exciton dissociation between donor and acceptor materials.

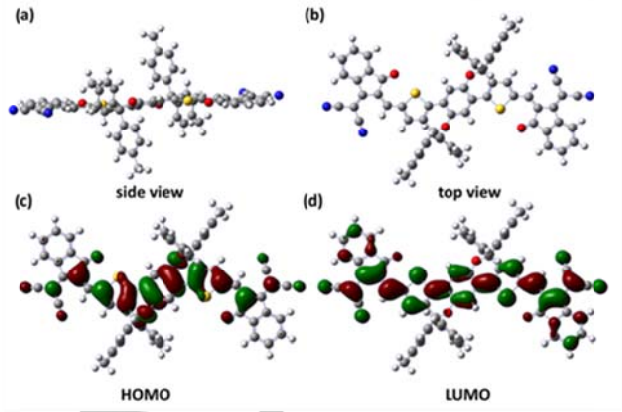

Figure 4. (a, b) The optimized geometry of PTIC; (c, d) Molecular orbitals of PTIC simulated with Gaussian B3LYP/6-31G(d, p).

DFT calculation

The molecular geometry and the frontier molecular orbitals of PTIC were simulated by density functional theory calculations with Gaussian 09 software at the B3LYP/6-31G(d,p) theory level. Long hexyl chains were replaced by methyl groups to facilitate the calculation. As shown in Figure 4, the backbone was nearly planar and the phenyl rings in side chains were almost perpendicular to the backbone. The coplanarity of backbone facilitates π-π stacking in solid state, while the steric hindrance between the side chains and the main backbone prevents severe aggregation. Compared to IDT core which is perfectly planar,[13,24] PDT unit showed a dihedral angle of 12.6° between the phenyl ring and thiophene ring as a result of introducing oxygen atoms. Besides, the thiophene ring in the PDT core and the IC group have a dihedral angle of 12.6°. The HOMO orbital delocalizes in the PDT core, while the LUMO orbital delocalizes in the whole backbone. The LUMO and HOMO levels were calculated to be -3.42 eV and -5.58 eV, giving an energy gap of 2.16 eV.

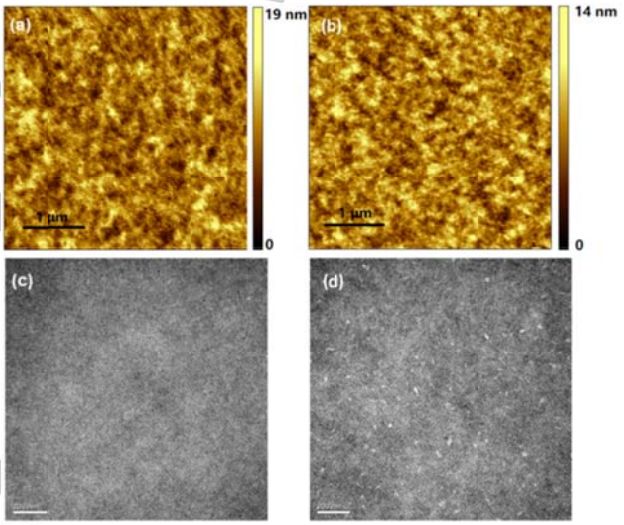

Figure 5. AFM height images (a, b) and TEM images (c, d) of PBDB-T:PTIC (1:1) blend film without (a, c) and with (b, d) thermal annealing at 160 °C.

Morphology

The morphology of active blend was illustrated by AFM and TEM images. As the shown in AFM images (Figure 5), the blend film with and without thermal annealing showed similar and smooth morphology with RMS values of 2.3 and 1.7 nm respectively, uniformly covering the entire scan area. There was no obvious phase separation, suggesting good miscibility between PTIC and PBDB-T. In contrast, the TEM image of the blend film with thermal annealing revealed the crystalline grains which were not observed in blend film without thermal annealing. In TEM images, the bright regions are polymer-rich domains and the dark regions are acceptor-rich domains. Apparently, the polymer donor exhibited enhanced crystallinity in blend film processed with thermal annealing. The crystalline domains facilitated charge transport and were beneficial for obtaining high charge mobilities. Besides, the pure domains reduced geminate recombination. In addition, the crystalline domains were still in

nanometer scale around 20-30 nm, which would not hamper charge separation.

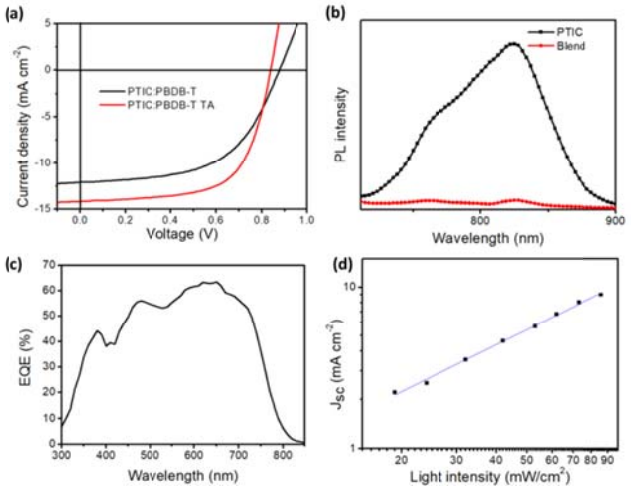

Figure 6. (a) *J-V* curves for the device based on PBDB-T:PTIC; (b) Photoluminescence (PL) spectra of PTIC and blend film of PBDB-T:PTIC (1:1) excited at 650 nm; (c) EQE spectra for PSCs based on PBDB-T:PTIC active layer processed by thermal annealing (TA); (d) dependence of J_{SC} on light intensity.

Photovoltaic properties

The photovoltaic properties of PTIC were investigated by fabricating conventional solar cell devices with architecture of ITO/PEDOT:PSS/PBDB-T:PTIC/Ca/Al. The detailed process of devices optimization was shown in Table S3 (Supporting Information). The highest PCE was achieved with a donor/acceptor ratio of 1:1 from CB solution under thermal annealing at 160 °C, as shown in Figure 6a and Table 2. The solar cells based on the optimized PBDB-T:PTIC active layer exhibited a maximum PCE of 7.66% with V_{OC} of 0.84 V, J_{SC} of 14.2 mA cm^{-2}, and FF of 0.64. Compared to the devices without annealing which exhibited a maximum PCE of 5.89% with V_{OC} of 0.88 V, J_{SC} of 12.1 mA cm^{-2}, and FF of 0.55, the annealed one showed much higher J_{SC} and FF, indicating lower charge recombination. The photoluminescence quenching spectra of neat PTIC and blend film were examined to confirm the exciton dissociation in the blends, as shown in Figure 6b. By blending PBDB-T into PTIC, an effective PL quenching (~92%) could be observed, indicating efficient exciton dissociation at the donor-acceptor interface.

The external quantum efficiency (EQE) curves of the best devices based on PTIC are shown in Figure 6c. The devices exhibit a broad photo-response from 300 to 800 nm with a highest response of 65%, indicating the donor and acceptor made complementary contribution to photocurrent generation.

To investigate charge recombination behaviors in the active layer of PSC devices, J_{SC} under different light-intensity (P_{light}) was measured (Figure 6d). The dependence of J_{SC} on light intensity can be described by the formula, $J_{SC} \propto P_{light}^{\alpha}$. Power-law exponent α is consistent with the extent of bimolecular recombination. The value of α in annealed PBDB-T:PTIC blend was 0.97, which indicates that there is weak bimolecular recombination in the blend film.

To investigate the charge transport properties of PTIC, electron and hole mobility were measured by space-charge-limited current (SCLC) method with hole-only device configuration of ITO/PEDPOT:PSS/PBDB-T:PTIC/Au and electron-only device configuration of ITO/ZnO/PBDB-T:PTIC/Ca/Al (Figure S3). The electron and hole mobility of the blend without annealing were determined to be 1.03×10^{-5} and 1.55×10^{-5} cm^2 V^{-1} s^{-1}, respectively. By thermal annealing, the electron and hole mobility of the blend significantly increased to 4.88×10^{-5} and 9.29×10^{-5} cm^2 V^{-1} s^{-1}, which was 4.7 times and 6 times of that without thermal annealing, respectively. Higher improvement in hole mobility than that of electron mobility was in accordance with higher crystallinity of polymer donors in blend observed by TEM. The thermal annealing is in favor of improving crystallinity and molecular packing in the blend film, which is beneficial for improving charge mobility and reducing charge recombination. As a result, the J_{SC} and FF are both increased with thermal annealing.

Conclusions

We designed and synthesized a novel ladder type backbone (PDT) for constructing an A-D-A type nonfullerene acceptor for PSCs. PDT has a nearly planar structure and it exhibits slip stacking in crystals. Compared with the commonly used IDT core, PDT exhibited stronger electron-donating properties. With PDT as the core structure, a new acceptor PTIC was synthesized and it shows broadened and red-shifted absorption compared to the corresponding IDT-based molecules. PSCs devices based on PBDB-T: PTIC exhibited a maximum PCE of 7.66%, with V_{OC} of 0.84 V, J_{SC} of 14.2 mA cm^{-2}, and FF of 0.64. The introduction of oxygen atoms would be an important strategy for the design of acceptors with wide absorption.

Table 2. The photovoltaic parameters of the devices based on PBDB-T:PTIC (1:1) under illumination of AM 1.5G, 100 mW cm^{-2}

Donor:acceptor	TA[a]	V_{OC} [V]	J_{SC} [mA cm^{-2}]	FF [%]	PCE[b] [%]	μ_e [cm^2 V^{-1} s^{-1}]	μ_h [cm^2 V^{-1} s^{-1}]
PBDB-T:PTIC	No	0.88	12.1	55	5.89 (5.68)	1.03×10^{-5}	1.55×10^{-5}
	Yes	0.84	14.2	64	7.66 (7.48)	4.88×10^{-5}	9.29×10^{-5}

[a] Thermal annealed at 160 °C for 10 min; [b] Average PCE values obtained from 10 devices are shown in parentheses.

Experimental Section

Materials synthesis. The syntheses of PTIC and experimental details can be found in the Supporting Information. PBDB-T was synthesized according to the previously reported literature precedure.[41] Unless otherwise stated, all chemicals were commercially available and were used without further purification.

Device fabrication and measurement. The organic solar cells devices were fabricated with a conventional architecture of ITO/PEDOT:PSS/PBDB-T:PTIC/Ca/Al. A solution of poly(3,4-ethylenedioxythiophene):poly(styrenesulfonate) (PEDOT:PSS, 30 nm) was spin-cast on pre-cleaned ITO coated glass at 4000 rpm and baked at 150 °C for 15 min in air, then the device was transferred into glovebox, where the active layer (100 nm) of the PBDB-T:PTIC solution in chlorobenzene was spin coated on the PEDOT:PSS layer. Finally, a Ca (10 nm)/Al (100 nm) metal top electrode was thermal evaporated onto the active layer under about 2×10^{-4} Pa. The active area of the device was 0.1 cm^2 defined by shadow mask. The current density-voltage (*J-V*) characteristics were measured with a Keithley 2420 source measurement unit under simulated 100 mW/cm^2 (AM 1.5 G) irradiation from a Newport solar simulator. Light intensity was calibrated with a standard silicon solar cell. The external quantum efficiencies (EQE) of solar cells were analyzed using a certified Newport incident photon conversion efficiency (IPCE) measurement system. Hole mobility and electron mobility were measured using the space charge limited current (SCLC) method with device configuration of ITO/PEDOT:PSS/polymer/Au and ITO/ZnO/PBDB-T:PTIC/Ca/Al by taking current-voltage in the range of 0-5 V. In the presence of carrier traps in the active layer, a trap filled-limit (TFL) region exists between the ohmic and trap-free SCLC regions.

CCDC 1572606 contains the supplementary crystallographic data for this paper. These data can be obtained free of charge from The Cambridge Crystallographic Data Centre via www.ccdc.cam.ac.uk/data_request/cif.

Acknowledgements

This work was supported by Ministry of Science and Technology of China (2016YFE0115000, 2014CB643501), National Natural Science Foundation of China (21202181, 51573205 and 51773220), Department of Science and Technology of Shandong Province (2015GGX104007, ZR2017ZB0314).

Keywords: non-fullerene polymer solar cells • small molecular acceptor • structure-property relationship • molecular packing

[1] G. Li, R. Zhu, Y. Yang, *Nat. Photon.*, **2012**, *6*, 153-161.
[2] Y. Li, *Acc. Chem. Res.*, **2012**, *45*, 723-733.
[3] C. Zhan, J. Yao, *Chem. Mater.*, **2016**, *28*, 1948-1964.
[4] C. B. Nielsen, S. Holliday, H.-Y. Chen, S. J. Cryer, I. McCulloch, *Acc. Chem. Res.*, **2015**, *48*, 2803-2812.
[5] (a) N. Liang, W. Jiang, J. Hou, Z. Wang, *Mater. Chem. Front.*, **2017**, *1*, 1291-1303. (b) Y. Cai, L. Huo, Y. Sun, *Adv. Mater.*, **2017**, *29*, 1605437.
[6] D. Zhu, X. Bao, Q. Zhu, C. Gu, M. Qiu, S. Wen, J. Wang, B. Shahid, R. Yang, *Energy Environ. Sci.*, **2017**, *10*, 614-620.
[7] Z. Liu, Y. Wu, Q. Zhang, X. Gao, *J. Mater. Chem. A*, **2016**, *4*, 17604-17622.
[8] Y. Lin, J. Wang, Z.-G. Zhang, H. Bai, Y. Li, D. Zhu, X. Zhan, *Adv. Mater.*, **2015**, *27*, 11701174.
[9] W. Zhao, S. Li, H. Yao, S. Zhang, Y. Zhang, B. Yang, J. Hou, *J. Am. Chem. Soc.*, **2017**, *139*, 7148-7151.
[10] (a) W. Li, H. Yao, H. Zhang, S. Li, J. Hou, *Chem.-Asian J.*, **2017**, *12*, 2160-2171. (b) T. Liu, Y. Guo, Y. Yi, L. Huo, X. Xue, X. Sun, H. Fu, W. Xiong, D. Meng, Z. Wang, F. Liu, T. P. Russell, Y. Sun, *Adv. Mater.*, **2016**, *28*, 10008-10015. (c) D. Meng, D. Sun, C. Zhong, T. Liu, B. Fan, L. Huo, Y. Li, W. Jiang, H. Choi, T. Kim, J. Y. Kim, Y. Sun, Z. Wang, A. J. Heeger, *J. Am. Chem. Soc.*, **2016**, *138*, 375-380. (d) T. Liu, X. Pan, X. Meng, Y. Liu, D. Wei, W. Ma, L. Huo, X. Sun, T. H. Lee, M. Huang, H. Choi, J. Y. Kim, W. C. H. Choy, Y. Sun, *Adv. Mater.*, **2017**, *29*, 1604251.
[11] (a) F. Liu, Z. Zhou, C. Zhang, J. Zhang, Q. Hu, T. Vergote, F. Liu, T. P. Russell, X. Zhu, *Adv. Mater.*, **2017**, *29*, 1606574. (b) X. Zhan, W. Xiong, Y. Gong, T. Liu, Y. Xie, Q. Peng, Y. Sun, Z. Li, *Solar RRL.*, **2017**, *1*, 1700123.
[12] Y. Lin, F. Zhao, Y. Wu, K. Chen, Y. Xia, G. Li, S. K. K. Prasad, J. Zhu, L. Huo, H. Bin, Z.-G. Zhang, X. Guo, M. Zhang, Y. Sun, F. Gao, Z. Wei, W. Ma, C. Wang, J. Hodgkiss, Z. Bo, O. Inganäs, Y. Li, X. Zhan, *Adv. Mater.*, **2017**, *29*, 1604155.
[13] Y. Wu, H. Bai, Z. Wang, P. Cheng, S. Zhu, Y. Wang, W. Ma, X. Zhan, *Energy Environ. Sci.*, **2015**, *8*, 3215-3221.
[14] T. Li, J. Wang, H. Chen, P. Cheng, S. Huang, Y. Lin, H. Yu, X. Zhan, *Dyes Pigm.*, **2017**, *137*, 553-559.
[15] Y. Lin, Z.-G. Zhang, H. Bai, J. Wang, Y. Yao, Y. Li, D. Zhu, X. Zhan, *Energy Environ. Sci.*, **2015**, *8*, 610-616.
[16] Y. Lin, J. Wang, T. Li, Y. Wu, C. Wang, L. Han, Y. Yao, W. Ma, X. Zhan, *J. Mater. Chem. A*, **2016**, *4*, 1486-1494.
[17] H. Yao, L. Ye, J. Hou, B. Jang, G. Han, Y. Cui, G. M. Su, C. Wang, B. Gao, R. Yu, H. Zhang, Y. Yi, H. Y. Woo, H. Ade, J. Hou, *Adv. Mater.*, **2017**, *29*, 1700254.
[18] S. Dai, F. Zhao, Q. Zhang, T.-K. Lau, T. Li, K. Liu, Q. Ling, C. Wang, X. Lu, W. You, X. Zhan, *J. Am. Chem. Soc.*, **2017**, *139*, 1336-1343.
[19] (a) Q. Cao, W. Xiong, H. Chen, G. Cai, G. Wang, L. Zheng, Y. Sun, *J. Mater. Chem. A*, **2017**, *5*, 7451-7461. (b) D. Xie, T. Liu, W. Gao, C. Zhong, L., Huo, Z. Luo, K.. Wu, W. Xiong, F. Liu, Y. Sun, C. Yang, *Solar RRL.*, **2017**, *1*, 1700044.
[20] B. Kan, H. Feng, X. Wan, F. Liu, X. Ke, Y. Wang, Y. Wang, H. Zhang, C. Li, J. Hou, Y. Chen, *J. Am. Chem. Soc.*, **2017**, *139*, 4929-4934.
[21] J. Wang, W. Wang, X. Wang, Y. Wu, Q. Zhang, C. Yan, W. Ma, W. You, X. Zhan, *Adv. Mater.*, **2017**, DOI: 10.1002/adma.201702125.
[22] Y. Li, L. Zhong, B. Gautam, H.-J. Bin, J.-D. Lin, F.-P. Wu, Z. Zhang, Z.-Q. Jiang, Z.-G. Zhang, K. Gundogdu, Y. Li, L.-S. Liao, *Energy Environ. Sci.*, **2017**, *10*, 1610-1620.
[23] Mishra, A.; Keshtov, M.; Looser, A.; Singhal, R.; Stolte, M.; Wurthner, F.; Bauerle, P.; Sharma, G. D., *J. Mater. Chem. A*, **2017**, *5*, 14887-14897.
[24] Y. Li, X. Liu, F.-P. Wu, Y. Zhou, Z.-Q. Jiang, B. Song, Y. Xia, Z.-G. Zhang, F. Gao, O. Inganas, Y. Li, L.-S. Liao, *J. Mater. Chem. A*, **2016**, *4*, 5890-5897.
[25] F. Zhao, S. Dai, Y. Wu, Q. Zhang, J. Wang, L. Jiang, Q. Ling, Z. Wei, W. Ma, W. You, C. Wang, X. Zhan, *Adv. Mater.*, **2017**, *29*, 1700144.
[26] L. Ye, W. Zhao, S. Li, S. Mukherjee, J. H. Carpenter, O. Awartani, X. Jiao, J. Hou, H. Ade, *Adv Energy Mater.*, **2017**, *7*, 1602000.
[27] Z. Zhang, L. Feng, S. Xu, J. Yuan, Z.-G. Zhang, H. Peng, Y. Li, Y. Zou, *J. Mater. Chem. A*, **2017**, *5*, 11286-11293.
[28] B. Xiao, A. Tang, J. Yang, Z. Wei, E. Zhou, *ACS Macro Lett.*, **2017**, *6*, 410-414.
[29] Y.-Q.-Q. Yi, H. Feng, M. Chang, H. Zhang, X. Wan, C. Li, Y. Chen, *J. Mater. Chem. A*, **2017**, *5*, 17204-17210.
[30] J. Zhu, S. Li, X. Liu, H. Yao, F. Wang, S. Zhang, M. Sun, J. Hou, *J. Mater. Chem. A*, **2017**, *5*, 15175-15182.
[31] W. Gao, Q. An, R. Ming, D. Xie, K. Wu, Z. Luo, Y. Zou, F. Zhang, C. Yang, *Adv. Funct. Mater.*, **2017**, *27*, 1702194.
[32] Z. Kang, S.-C. Chen, Y. Ma, J. Wang, Q. Zheng, *ACS Appl. Mater. Interfaces*, **2017**, *9*, 24771-24777.

[33] Ma, Y.; Zhang, M.; Yan, Y.; Xin, J.; Wang, T.; Ma, W.; Tang, C.; Zheng, Q., *Chem. Mater.*, **2017**, *29*, 7942-7952.
[34] Y. Lin, Q. He, F. Zhao, L. Huo, J. Mai, X. Lu, C.-J. Su, T. Li, J. Wang, J. Zhu, Y. Sun, C. Wang, X. Zhan, *J. Am. Chem. Soc.*, **2016**, *138*, 2973-2976.
[35] J. Wang, S. Dai, Y. Yao, P. Cheng, Y. Lin, X. Zhan, *Dyes Pigm.*, **2015**, *123*, 16-25.
[36] H. Bai, Y. Wu, Y. Wang, Y. Wu, R. Li, P. Cheng, M. Zhang, J. Wang, W. Ma, X. Zhan, *J. Mater. Chem. A*, **2015**, *3*, 20758-20766.
[37] S. Yu, Y. Chen, L. Yang, P. Ye, J. Wu, J. Yu, S. Zhang, Y. Gao, H. Huang, *J. Mater. Chem. A*, **2017**, *5*, 21674-21678.
[38] P. E. Hartnett, A. Timalsina, H. S. S. R. Matte, N. Zhou, X. Guo, W. Zhao, A. Facchetti, R. P. H. Chang, M. C. Hersam, M. R. Wasielewski, T. J. Marks, *J. Am. Chem. Soc.*, **2014**, *136*, 16345-16356.
[39] S. Holliday, R. S. Ashraf, C. B. Nielsen, M. Kirkus, J. A. Röhr, C.-H. Tan, E. Collado-Fregoso, A.-C. Knall, J. R. Durrant, J. Nelson, I. McCulloch, *J. Am. Chem. Soc.*, **2015**, *137*, 898-904.
[40] W. Zhao, D. Qian, S. Zhang, S. Li, O. Inganäs, F. Gao, J. Hou, *Adv. Mater.*, **2016**, *28*, 4734-4739.
[41] D. P. Qian, L. Ye, M. J. Zhang, Y. R. Liang, L. J. Li, Y. Huang, X. Guo, S. Q. Zhang, Z. A. Tan, J. H. Hou, *Macromolecules*, **2012**, *45*, 9611-9617.

10.1002/cssc.201701917

Entry for the Table of Contents (Please choose one layout)

FULL PAPER

A ladder type molecule pyran-bridged indacenodithiophene (PDT) is designed to construct non-fullerene acceptor (PTIC) in polymer solar cell. The central structure of PDT exhibits an ordered molecular packing in the crystal. The introduction of oxygen increases the HOMO level and expands the absorption. PSC device based on PBDB-T:PTIC shows a power conversion efficiency of 7.66%.

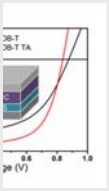

Shuguang Wen, Yao Wu, Yingying Wang, Yi Li, Ling Liu, Huanxiang Jiang, Zhitian Liu, Renqiang Yang**

Page No. – Page No.

Pyran-bridged indacenodithiophene: A novel building block for constructing efficient A-D-A type nonfullerene acceptor for polymer solar cells